JACS
JOURNAL OF THE AMERICAN CHEMICAL SOCIETY
Article
Cite This: J. Am. Chem. Soc. 2018, 140, 2595−2601
pubs.acs.org/JACS

Self-Sorting of Heteroanions in the Assembly of Cross-Shaped Polyoxometalate Clusters

Qi Zheng,[†] Laia Vilà-Nadal,[†] Zhongling Lang,[‡] Jia-Jia Chen,[†] De-Liang Long,[†] Jennifer S. Mathieson,[†] Josep M. Poblet,*[,‡] and Leroy Cronin*[,†]

[†]WestCHEM, School of Chemistry, The University of Glasgow, Glasgow G12 8QQ, United Kingdom
[‡]Departament de Química Física i Inorgànica, Universitat Rovira i Virgili, c/Marcel·lí Domingo 1, 43007 Tarragona, Spain

Supporting Information

ABSTRACT: Heteroanion (HA) moieties have a key role in templating of heteropolyoxometalate (HPA) architectures, but clusters templated by two different templates are rarely reported. Herein, we show how a cross-shaped HPA-based architecture can self-sort the HA templates by pairing two different guests into a divacant $\{XYW_{15}O_{54}\}$ building block, with four of these building block units being linked together to complete the cross-shaped architecture. We exploited this observation to incorporate HA templates into well-defined positions within the clusters, leading to the isolation of a collection of mixed-HA templated cross-shaped polyanions $[(XYW_{15}O_{54})_4(WO_2)_4]^{32-/36-}$ (X = H−P, Y = Se, Te, As). The template positions have been unambiguously determined by single crystal X-ray diffraction, NMR spectroscopy, and high-resolution electrospray ionization mass spectrometry; these studies demonstrated that the mixed template containing HPA clusters are the preferred products which crystallize from the solution. Theoretical studies using DFT calculations suggest that the selective self-sorting originates from the coordination of the template in solution. The cross-shaped polyoxometalate clusters are redox-active, and the ability of molecules to accept electrons is slightly modulated by the HA incorporated as shown by differential pulse voltammetry experiments. These results indicate that the cross-shaped HPAs can be used to select templates from solution, and themselves have interesting geometries, which will be useful in developing functional molecular architectures based upon HPAs with well-defined structures and electronic properties.

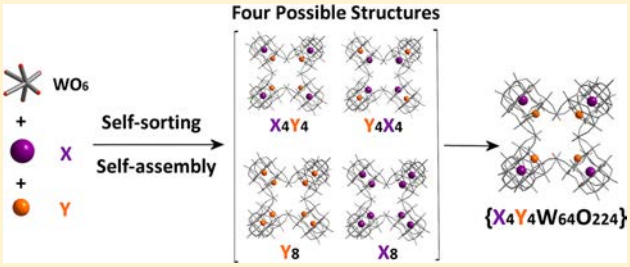

1. INTRODUCTION

Understanding, and in turn controlling, self-assembly and self-sorting in designed systems has been key to develop supramolecular chemistry,[1,2] molecular architectures, and functional-molecule-based devices.[3,4] This is because the ability to design using template control promises to not only result in novel chemical entities but also systems with increased complexity and functionality.[5−7] Polyoxometalate (POM) clusters are based on group 5 or 6 transition metals (V, Nb, Ta, Mo, and W) in their highest oxidation states, linked by oxygen atoms, which are most easily understood by viewing them as metal-oxo units where the metal ion defines the center of a polyhedral building block.[8,9] POMs are formed in aqueous conditions allowing the self-assembly of those metal-oxo building blocks, followed by elimination of water, as the pH in the solution is lowered. Two of the most remarkable properties of POMs are their high acidity and redox active character and also the fact that they can be assembled into inorganic frameworks by using electrophiles to connect the nodes.[10−12] As a result, POMs have possible applications in catalysis,[13−15] medicine,[16−18] and magnetism, but key studies are still fundamental and mechanistic in nature.[19−21] POMs are redox active[22,23] and able to reversibly store and transfer electrons making them promising candidates for electronically active molecule-based technologies.[24,25] Overall, POMs are a diverse family of molecular clusters[26,27] that span over a large range of nuclearities, from 6 to over 300 metal units, and dimensions, ranging from 1 to 5.6 nm.[28−32]

Given this diversity POMs are classified into three categories defined by their elemental composition, structure, and heteroatoms. These are isopolyoxometalates, heterpolyoxometalates, and highly reduced molybdenum blues and browns. Heteropolyanions (HPAs) result from combining metal-oxo building blocks with heteroanions (HAs), such as $[SO_4]^{2-}$, $[PO_4]^{3-}$, $[AsO_4]^{3-}$; this combination increases the stability of clusters and offers a wider range of applications. Hence, the inclusion of HAs has been widely explored in POM chemistry. These studies have mostly focused on the structure of the clusters and their composition, but the mechanism of assembly in solution is not known, especially for the more complex structures. Indeed, it is not known if it is possible to selectively include different HA templates into the HPAs,[8,31,33] although recent work has explored the inclusion of redox-active heteroanions[34,35] incorporated into the clusters.[36−42]

Received: November 11, 2017
Published: January 23, 2018

DOI: 10.1021/jacs.7b11982
J. Am. Chem. Soc. 2018, 140, 2595−2601

Scheme 1. Self-Sorting and Self-Assembly of Heteroanion Templated Nanoscale Cross-Shaped Polyoxoanions $[H_4P_4X_4W_{64}O_{224}]^{32-/36-}$ (X = Te, Se, As, P)[a]

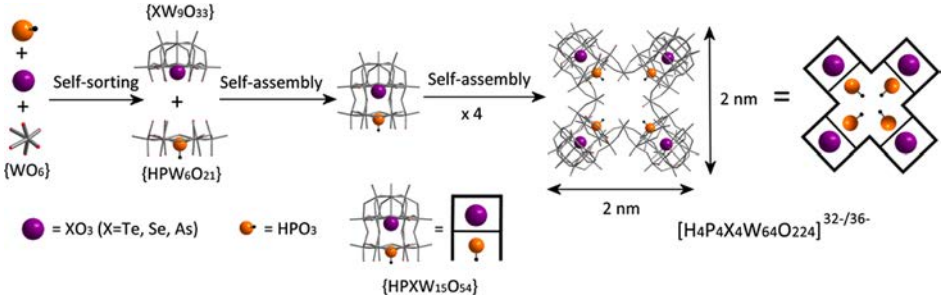

[a]Color scheme: purple and orange: heteroanions XO_3; grey: tungsten; red: oxygen; black: hydrogen.

The precise positioning of the HAs in the cluster shell remains as an open question, akin to the possibility of doping metal bulk oxides. In this work, we aimed to explore the positioning of mixed HAs within the clusters by including different types of HAs in solution, so that during the formation of the POM cluster, a number of different HAs are available to be included in the structure. However, POMs templated by two different types of HAs are rarely reported since it is difficult to structurally determine two different HAs coexisting in the same building block.[43−45] Furthermore, a fundamental understanding of how mixed HAs interact with building units and self-assemble into a well-defined architecture is still poorly understood.

In this paper, we describe the results obtained by allowing different types of HAs to be present under a range of different synthetic conditions, all of which aimed to produce HPA clusters. This is because we wondered how the system would cope with when two different types of pyramidal HAs are incorporated into a reaction, in this case: $[HPO_3]^{2-}$, $[TeO_3]^{2-}$, $[SeO_3]^{2-}$, and $[AsO_3]^{3-}$. To do this, we adapted the synthesis of the previously reported cross-shaped polyanion $[(Te_2W_{15}O_{54})_4(WO_2)_4]^{32-}$.[46] We chose this because the cross-shaped structure has four $\{(XO_3)_2W_{15}\}$ building blocks joined together by four $\{WO_6\}$ octahedral units, and therefore four chances to incorporate different HAs. The two $\{XO_3\}$ vacant sites in the $\{(XO_3)_2W_{15}\}$ building blocks are two structurally defined positions, namely a lacunary or capped position, for the HA self-sorting process to occur. $[HPO_3]^{2-}$ was chosen as the main HA to pair with $[TeO_3]^{2-}$, $[SeO_3]^{2-}$, and $[AsO_3]^{3-}$, respectively. The paired HAs were selected on the basis of their intrinsic electronic properties and their relative sizes, which would in principle facilitate differentiation and tune the electronic properties of the new clusters.

We found that the HA self-sorting approach was successful, and we were able to include two different HAs within the cluster architectures in two well-defined positions. The building blocks self-assembled into cross-shaped cluster architectures as intended, leading to a collection of mixed-HAs incorporated into the cross-shaped HPAs $[(XYW_{15}O_{54})_4(WO_2)_4]^{32-/36-}$ (X = H−P, Y = Se, Te, As) (Scheme 1). The HAs are self-sorted in a highly selective fashion, in terms of identity and position, and exhibit an interesting substitution preference. Density functional theory (DFT) calculations were carried out to investigate the driving force for the selective substitution, thereby depicting a potential pathway for the controlled self-assembly of a given structure type as a function of the different HAs available in solution. Electrochemical experiments and electron paramagnetic resonance (EPR) spectroscopy showed that the compounds are electronically active.

2. EXPERIMENTAL METHODS

General Materials. $Na_2WO_4{\cdot}2H_2O$ (Sigma-Aldrich, ≥99%), H_3PO_3 (Sigma-Aldrich, 99%), Na_2TeO_3 (Sigma-Aldrich, 99%), Na_2SeO_3 (Sigma, 99%), $NaAsO_2$ (Sigma-Aldrich, ≥90%), HCl (Sigma, analytical grade, 36.5%−38% aqueous solution), $(CH_3)_2NH_2Cl$ (Sigma-Aldrich, 98+%). All chemicals were used as received.

Synthesis of $(C_2H_8N)_{13}Na_{19}[H_4P_4Te_4W_{64}O_{224}]{\cdot}30H_2O$ ***(Te$_4$P$_4$)***. $Na_2WO_4{\cdot}2H_2O$ (3.4 g, 10.3 mmol), Na_2TeO_3 (0.13 g, 0.6 mmol), H_3PO_3 (0.05 g, 0.6 mmol), and dimethylamine hydrochloride (0.7 g, 8.6 mmol) were dissolved in water (30 mL). The pH was first adjusted to 6.0 by addition of 50% acetic acid and then further to 4.0 by 37% HCl. The solution was heated at 60 °C for 50 min, then filtered at room temperature, and left to evaporate slowly. Colorless needle-shaped crystals appeared after 1 week. Yield: 36.0% (based on P). Characteristic IR bands (cm^{-1}): 3433(b), 3151(b), 2777(w), 2364(w), 1624(m), 1462(w), 1404(w), 1072(s), 948(w), 798(s), 713(s), 644(m). Elemental analysis for $C_{26}H_{168}N_{13}Na_{19}O_{254}P_4Te_4W_{64}$: M_W = 17564.97 g mol^{-1}, calcd (%): W 67.0, P 0.7, Te 2.9, H 1.0, C 1.8, N 1.0, Na 2.5; found: W 69.8, P 0.7, Te 3.7, H 0.8, C 1.8, N 1.0, Na 2.7. Calculated TGA water loss from 25 to 450 °C (%) calcd: 3.1, found 3.8.

Synthesis of $(C_2H_8N)_{23}Na_9[H_4P_4Se_4W_{64}O_{224}]{\cdot}30H_2O$ ***(Se$_4$P$_4$)***. $Na_2WO_4{\cdot}2H_2O$ (9.5 g, 28.8 mmol), H_3PO_3 (0.08 g, 1.0 mmol), sodium selenite (0.25 g, 1.4 mmol), and dimethylamine hydrochloride (DMA·HCl) (3.5 g, 42.9 mmol) were dissolved in 30 mL water. Diluted hydrochloric acid (6 M) was added dropwise under stirring, and the pH was adjusted to 3.2. The solution was heated around 40 °C, with stirring until it become cloudy. After cooling down to room temperature, a white powder formed and was removed by filtration. Colorless needle-shaped crystals were isolated from the filtrate after 4 days. Yield: 6.2% (based on P). Characteristic IR bands (cm^{-1}): 3439(b), 3152(b), 2779(m), 2434(w), 1624(m), 1465(m), 1249(w), 1078(s), 1018(w), 949(s), 889(s), 792(s), 640(w). Elemental analysis for $C_{46}H_{248}N_{23}Na_9O_{254}P_4Se_4W_{64}$: M_W = 17601.44 g mol^{-1}, calcd (%): W 66.8, P 0.7, Se 1.8, H 1.4, C 3.1, N 1.8, Na 1.2%; found (%): W 66.1, P 0.6, Se 1.8, H 1.2, C 3.2, N 1.9, Na 1.1. Calculated TGA water loss from 25 to 450 °C (%) calcd: 3.1, found 3.7.

Synthesis of $(C_2H_8N)_{19}Na_{17}[H_4P_4As_4W_{64}O_{224}]{\cdot}25H_2O$ ***(As$_4$P$_4$)***. $Na_2WO_4{\cdot}2H_2O$ (3.75 g, 11.4 mmol), $NaAsO_2$ (0.13 g, 1.0 mmol), H_3PO_3 (0.04 g, 0.49 mmol), and dimethylamine hydrochloride (1.75 g, 21.5 mmol) were dissolved in water (15 mL). Diluted hydrochloric acid (6 M) was added dropwise under stirring, and the pH was adjusted to 4.3. The solution was heated at 60 °C for 35 min, and then the solution was filtered at room temperature and left to evaporate slowly. Colorless crystals were isolated after 2 weeks. Yield: 9.3% (based on P). Characteristic IR bands (cm^{-1}): 3419(b), 3124(b), 3032(b), 2767(w), 2401(w), 1627(m), 1458(w), 1083(s), 949(w), 875(m), 790(s), 711(s), 624(m). Elemental analysis for

DOI: 10.1021/jacs.7b11982
J. Am. Chem. Soc. 2018, 140, 2595−2601

$C_{38}H_{206}As_4N_{19}Na_{17}O_{249}P_4W_{64}$: M_W = 17494.76 g mol^{-1}, calcd (%): W 67.2, P 0.7, As 1.7, H 1.2, C 2.6, N 1.5, Na 2.2; found (%): W 66.7, P 0.7, As 1.5, H 1.3, C 3.3, N 1.8, Na 1.3. Calculated TGA water loss from 25 to 450 °C (%) calcd: 5.4, found 5.3.

Synthesis of $(C_2H_8N)_{15}Na_{17}[H_8P_8W_{64}O_{224}]\cdot 30H_2O$ (P_8). $Na_2WO_4\cdot 2H_2O$ (5.5 g, 16.7 mmol), H_3PO_3 (0.20 g, 2.4 mmol), and dimethylamine hydrochloride (DMA·HCl) (1.5 g, 18.4 mmol) were dissolved in 20 mL water. Diluted hydrochloric acid (6 M) was added dropwise under stirring, and the pH was adjusted to a pH value of 2.7. The solution was heated to around 40 °C, with stirring until it become cloudy. After cooling down to room temperature, a white powder formed and was removed by filtration. Colorless block crystals were isolated from the filtrate after 2−3 weeks. Yield: 6.9% (based on W). Characteristic IR bands (cm^{-1}): 3437(b), 3149(b), 2774(w), 2360(w), 1623(m), 1463(m), 1075(s), 949(s), 863(s), 795(s), 721(s), 650(w). Elemental analysis for $C_{30}H_{188}N_{15}Na_{17}O_{254}W_{64}P_8$: M_W = 17228.71 g mol^{-1}, calcd (%): W 68.3, P 1.4, H 1.1, C 2.1, N 1.2, Na 2.3; found (%): W 63.7, P 1.4, H 1.0, C 2.1, N 1.2, Na 2.7. Calculated TGA water loss from 25 to 450 °C (%) calcd: 3.1, found 3.8.

3. RESULTS AND DISCUSSION

3.1. Self-Sorting of Mixed HAs into the Cross-Shaped Polyoxoanions. The HAs $[HPO_3]^{2-}$ and $[TeO_3]^{2-}$ were mixed in a similar way to the reported synthetic procedure for the cross-shaped $[W_{64}O_{200}(TeO_3)_8]^{32-}$.[46] This led to the isolation of the mixed $[TeO_3]^{2-}$ and $[HPO_3]^{2-}$ templated polyanion $[W_{64}O_{200}(HPO_3)_4(TeO_3)_4]^{32-}$ (**Te_4P_4**), which crystallized from the reaction. Single crystal X-ray diffraction analysis showed that **Te_4P_4** has D_{2d} symmetry. As shown in Figure 1, the **Te_4P_4** cluster consists of four $\{HPTeW_{15}\}$ building blocks connected by four octahedra $\{WO_6\}$ *via cis*-oxygen atoms. Each $\{HPTeW_{15}\}$ has a $\{W_3O_6\}$ cap and two $\{W_6O_{18}\}$ rings templated by $[TeO_3]^{2-}$ and $[HPO_3]^{2-}$, respectively.

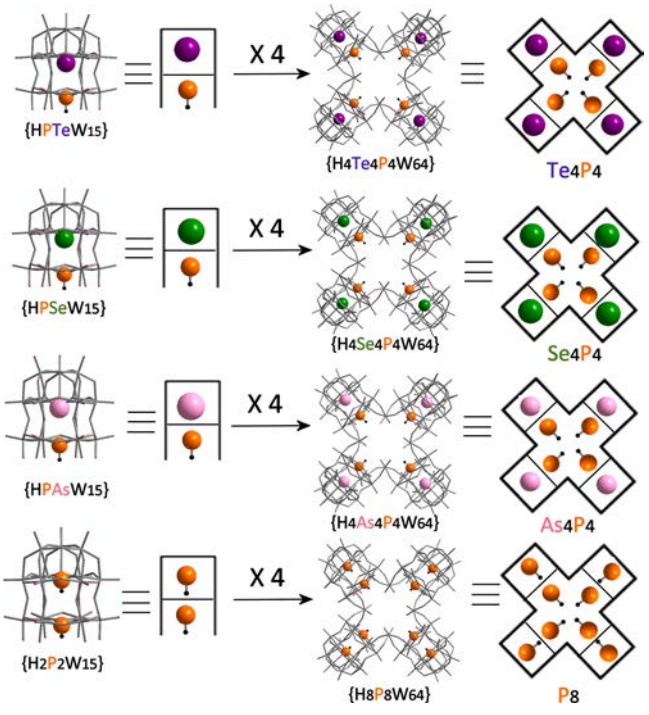

Figure 1. Structural representations of the $\{W_{15}\}$ building block of the four cross-shaped POMs **Te_4P_4**, **Se_4P_4**, **As_4P_4**, and **P_8**. Color scheme: Purple: tellurium; green: selenium; pink: arsenic; orange: phosphorus; gray: tungsten; red: oxygen; black: hydrogen.

The two $\{W_6O_{18}\}$ rings are joined together through six corner-sharing oxygen ligands. The two HAs were unambiguously determined as $[TeO_3]^{2-}$ and $[HPO_3]^{2-}$, respectively, through single crystal X-ray data. This was possible due to their different electron densities and their atomic sizes, that is, Te−O and P−O bond lengths are 1.90 and 1.50 Å, respectively. In our system, the self-sorting process seemed to operate counter to conventional steric considerations. This is because the smaller $[HPO_3]^{2-}$ moiety, with its small size, is found at the uncapped end of $\{W_{15}\}$, whereas the $[TeO_3]^{2-}$ moiety, with its larger size, is found to be located at the more sterically hindered capped end which has a smaller cavity (see Figure 1).

In order to gain a better understanding of how the HAs are selectively self-sorted into the $\{XYW_{15}\}$ vacancies and also to investigate if **Te_4P_4** is the only example containing two different HAs in the structure, reactions with complementary pairs of $[SeO_3]^{2-}/[HPO_3]^{2-}$ and $[AsO_3]^{3-}/[HPO_3]^{2-}$ were also conducted. Structural analysis shows that all the reactions led to the isolation of cross-shaped structures templated by two different types of HAs in the $\{W_{15}\}$ building units, including $[W_{64}O_{200}(SeO_3)_4(HPO_3)_4]^{32-}$ (**Se_4P_4**) and $[W_{64}O_{200}(AsO_3)_4(HPO_3)_4]^{36-}$ (**As_4P_4**) in addition to the $[W_{64}O_{200}(TeO_3)_4(HPO_3)_4]^{32-}$ (**Te_4P_4**). All of the HAs in those structures are well identified according to X-ray data (Tables S1 and S2), and **Se_4P_4** and **As_4P_4** show a consistent preference of HA substitution as found in the structure of **Te_4P_4**. Also, as a control, we synthesized the pure phosphite incorporated cross-shaped compound $[W_{64}O_{200}(HPO_3)_8]^{32-}$ (**P_8**).

To understand the self-sorting of two different templates within the $\{W_{15}\}$ moieties from a structural point of view, special attention was paid to $[HPO_3]^{2-}$ as it contains a proton in contrast to the other $[XO_3]^{2-/3-}$ (X = Se, Te, As) templates (Figure 1). In the structural determination, the H atom located on the phosphorus center is geometrically generated and then refined with P−H bond length being fixed to 1.42 Å based upon the bond length of free phosphite. The presence of a proton on phosphite, other than lone pair, leads to the $[HPO_3]^{2-}$ moiety to adopt a tetrahedral configuration, as indicated by the average O−P−O angle of 110.0°, which is quite close to that found for the ideal tetrahedral bond angle. On the contrary, the lone pair on $[SeO_3]^{2-}$, $[TeO_3]^{2-}$, and $[AsO_3]^{3-}$ exerts more electrostatic repulsion to the X−O bonds than the P−H σ bond, thus forcing the X−O bonds to deviate from the ideal tetrahedral arrangement around central X atoms. Indeed, the average O−X−O angles in these HAs are 92.0° ($[TeO_3]^{2-}$), 98.4° ($[SeO_3]^{2-}$), 95.9° ($[AsO_3]^{3-}$), respectively. Therefore, it is quite clear that they should all adopt trigonal pyramidal shape as observed. This may account for the different position of two HAs in $\{W_{15}\}$ building blocks. Further, in principle, the tetrahedral $[HPO_3]^{2-}$ moiety requires more space so that the P−H unit can be accommodated into the cluster and therefore explains why it is located at the uncapped end of $\{W_{15}\}$, while the other $[XO_3]^{2-/3-}$ moieties are being accommodated at the capped end.

In addition to extensive structural analysis using single crystal X-ray crystallography, the positions of the HAs within the metal oxide cluster have also been unambiguously identified through nuclear magnetic resonance (NMR) spectroscopy (Figure 2) and electrospray ionization mass spectrometry (ESI-MS) (Figure 3 and Figures S1−S9). As is shown in Figure 2, the ^{31}P NMR of **P_8** exhibits two doublets with two distinct $\{^{31}P\}$-$\{^1H\}$ coupling constants, $^1J_{PH}$ = 779 Hz and $^1J_{PH}$ = 727 Hz,

DOI: 10.1021/jacs.7b11982
J. Am. Chem. Soc. 2018, 140, 2595−2601

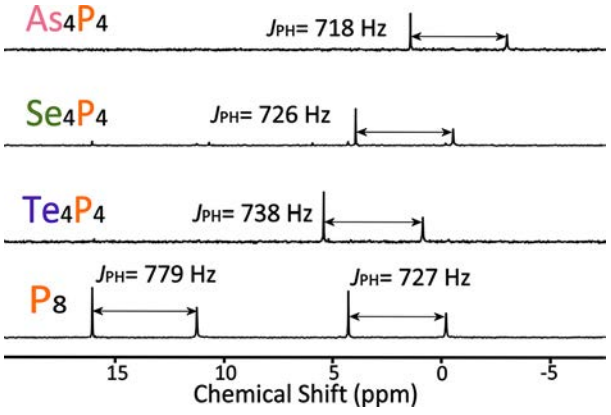

Figure 2. ^{31}P NMR spectra of $[W_{64}O_{200}(HPO_3)_8]^{32-}$ (**P_8**) in 1 M NaCl/D_2O solution showing two doublets with $^1J_{PH}$ = 727 Hz and $^1J_{PH}$ = 779 Hz; $[W_{64}O_{200}(TeO_3)_4(HPO_3)_4]^{32-}$ (**Te_4P_4**) in D_2O solution showing a doublet with $^1J_{PH}$ = 738 Hz; $[W_{64}O_{200}(SeO_3)_4(HPO_3)_4]^{32-}$ (**Se_4P_4**) in 1 M NaCl/D_2O solution showing a doublet with $^1J_{PH}$ = 726 Hz; $[W_{64}O_{200}(AsO_3)_4(HPO_3)_4]^{36-}$ (**As_4P_4**) in 1 M LiCl/D_2O solution showing a doublet with $^1J_{PH}$ = 718 Hz.

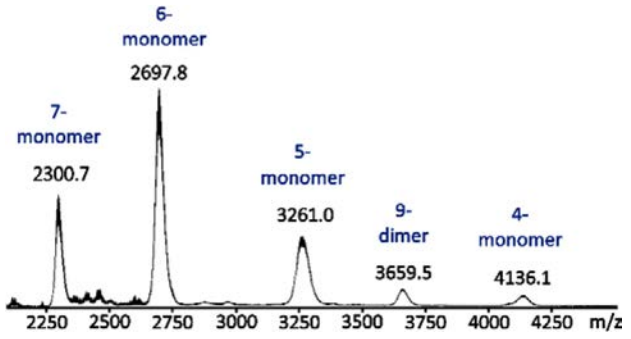

Figure 3. ESI-MS spectra of **Te_4P_4** in water/acetonitrile (5%:95%) mixture solvent.

suggesting two phosphorus-based species are located within the $\{W_{15}\}$ building units. The downfield doublet can be assigned to the phosphorus occupying the capped end of $\{W_{15}\}$ due to the stronger shielding effects from the tungsten oxide shell. In contrast, the compounds **Te_4P_4**, **Se_4P_4**, and **As_4P_4** only each exhibit one doublet located at high field in ^{31}P NMR. This doublet indicates there is only one type of phosphorus within the structures, and they are all located at the uncapped-end of the $\{W_{15}\}$ units. Furthermore, the proton decoupled ^{31}P NMR shows that all the doublets in ^{31}P NMR are now merged into singlets. These singlets indicate the protonation of phosphorus-based HAs in all compounds (Figure S1). The ^{1}H NMR in Figures S3 and S4 also confirm this assignment. However, the individual lines in doublets in the ^{31}P NMR spectra for all these four compounds have different intensities. The upfield line is broadened and therefore appears less intense, although the experiment with proton decoupling shows that these two lines are indeed part of a phosphorus-proton doublet. The difference in the line widths can be explained by "relaxation interference", which originates from the interaction between dipole−dipole (DD) and chemical shift anisotropy (CSA) relaxation. This effect is commonly seen in large biomolecules, such as proteins due to their large size leading to slow tumbling in the solution.[47,48] In our case, the cross-shaped POM architype measures 2 nm × 2 nm in length and width and its molecular weight is ca. 17 kDa, therefore the line broadening is very prominent. This observation is confirmed by undertaking ^{31}P NMR at 343 K; here much less differences between line intensities were observed due to decreased contribution of the CSA relaxation (Figure S5). **Te_4P_4** and **Se_4P_4** were also further analyzed by ^{125}Te and ^{77}Se NMR to confirm the presence of the HA templates. Also, the ^{125}Te NMR of **Te_4P_4** showed a sharp singlet at δ= 1792 ppm corresponding to the tellurium species in the cross-shaped anion (Figure S5). Similarly, the existence of SeO_3 in **Se_4P_4** is indicated by the sharp singlet found at 1314 ppm in ^{77}Se NMR spectrum (Figure S6). However, it should be noted that some minor signals corresponding to **P_8** were also observed in the ^{31}P NMR of **Se_4P_4**, indicating $[SeO_3]^{2-}$ and $[HPO_3]^{2-}$ are competing with each other during the self-sorting process. Therefore, based on the NMR analysis, we can conclude that the different types of HAs can be selectively added into the cross-shaped structure and the mixed-HA incorporated compounds are the preferred self-sorting products crystallizing from the reaction.

ESI-mass spectrometry was employed to analyze the solution behavior of obtained clusters (Figure 3). In the case of **Te_4P_4**, intact molecular species could be detected at m/z 2300.7 for $[W_{64}O_{200}(HPO_3)_4(TeO_3)_4H_{21}Na_4]^{7-}$, 2697.8 for $[W_{64}O_{200}(HPO_3)_4(TeO_3)_4H_{18}Na_8]^{6-}$, 3261.0 for $[W_{64}O_{200}(HPO_3)_4(TeO_3)_4(C_2H_8N)_6NaH_{20}]^{5-}$, and 4136.1 for $[W_{64}O_{200}(HPO_3)_4(TeO_3)_4Na_{24}H_4]^{4-}$. In addition, a dimeric species was also observed at m/z 3659.5 for $[(W_{64}O_{200}(HPO_3)_4(TeO_3)_4)_2(C_2H_8N)_{31}NaH_{23}]^{9-}$. Similarly, integral species of **Se_4P_4**, **As_4P_4**, and **P_8** were also observed via mass spectrometry (Figures S7−S9, Tables S3−S6), suggesting the cross-shaped clusters are stable in solution.

3.2. Computational Implications of Driving Force for Highly Selective HA Self-Sorting. Density functional theory (DFT) calculations were carried out to understand the driving force behind the observed HA-driven self-sorting process. Initially, geometry optimizations were performed for the cross-shaped polyanions (**Te_4P_4**, **Se_4P_4**, and **As_4P_4**) and their isomeric structures (**Te_4P_4'**, **Se_4P_4'**, and **As_4P_4'**) by inverting the position of the $[HPO_3]^{2-}$ unit. The main structural parameters, and in particular the X-P distances, elucidated using X-ray diffraction studies were reproduced by the DFT calculations. Hence, the computed X−P distances (Å) are dependent on the heteroatom X, as shown by computed DFT and X-ray data (in parentheses): Te−P = 3.66 (3.64), Se−P = 3.78 (3.80), and As−P= 3.79 (3.80). We also explored the relative stability of **Te_4P_4**-**Te_4P_4'**, **Se_4P_4**-**Se_4P_4'**, and **As_4P_4**-**As_4P_4'** pairs. As shown in Table 1, all the structures with

Table 1. Relative Energies for Cross-Shaped Anions with $[HPO_3]^{2-}$ Unit Occupying Capped and Uncapped Ends of the Building Blocks[a]

polyanions	$[HPO_3]^{2-}$ location	ΔE	building block $\{XYW_{15}\}$	ΔE
P_4Te_4	uncapped	0.0	$\{PTeW_{15}\}$	0.0
P_4Te_4'	capped	24.7	$\{PTeW_{15}\}'$	8.1
P_4Se_4	uncapped	0.0	$\{PSeW_{15}\}$	0.0
P_4Se_4'	capped	6.2	$\{PSeW_{15}\}'$	2.7
P_4As_4	uncapped	0.0	$\{PAsW_{15}\}$	0.0
P_4As_4'	capped	42.6	$\{PAsW_{15}\}'$	7.4

[a]Energies are in kcal·mol^{-1}; $[HPO_3]^{2-}$ unit occupies alternatively uncapped and capped positions in cross-shaped anions represented in Figure 1.

DOI: 10.1021/jacs.7b11982
J. Am. Chem. Soc. 2018, 140, 2595−2601

$[HPO_3]^{2-}$ occupying the uncapped/lacunary end ($\mathbf{Te_4P_4}$, $\mathbf{Se_4P_4}$, $\mathbf{As_4P_4}$) are significantly more stable than when it is located on the capped ($\mathbf{Te_4P_4}'$, $\mathbf{Se_4P_4}'$, $\mathbf{As_4P_4}'$) end, with energy differences of 24.7, 6.2, and 42.6 kcal·mol^{-1} respectively. Only in the case of the $[HPO_3]^{2-}/[SeO_3]^{2-}$ pair did we find some competition between the $\mathbf{Se_4P_4}$ and $\mathbf{Se_4P_4}'$ since the two isomers differ in only 6.2 kcal·mol^{-1}. However, for the other two pairs, the occupation of the Te, and especially the As unit, in the capped end is of a much lower energy. Given that building blocks $\{HPTeW_{15}\}$ ($\mathbf{Te_4P_4}$, $\mathbf{Te_4P_4}'$), $\{HPSeW_{15}\}$ ($\mathbf{Se_4P_4}$, $\mathbf{Se_4P_4}'$), and $\{HPAsW_{15}\}$ ($\mathbf{As_4P_4}$, $\mathbf{As_4P_4}'$) show the same stability trends as the overall structures (see Table 1 and Figure S11), we performed an energy decomposition analysis using the building block anions to understand the role of the $[XO_3]^{2-}$ group in the formation of one or another species.[49] The interaction energy between $XO_3^{2-/3-}$ (X = H–P^{III}, Se^{IV}, Te^{IV}, and As^{III}) and the $[(HPO_3)W_{15}O_{51}]^{8-}$ building block (with $[HPO_3]^{2-}$ occupying the uncapped end) was decomposed. As expected, the total bonding energy (ΔE_B) is highly positive in all cases due to the anionic character of the two interacting fragments (Table 2).

Table 2. Interaction Energy Decomposition Analysis between XO_3^{q-} and $[(HPO_3)W_{15}O_{51}]^{8-}$ Units[a]

q−	XO_3	ΔE_B	ΔE_{SR}	ΔE_{OI}	ΔE_{sol}	$\Delta E_B + \Delta E_{sol}$
2−	TeO_3	483.9	806.3	−322.4	−578.2	−94.3
	SeO_3	523.6	785.2	−261.6	−595.4	−71.8
	HPO_3	536.5	766.2	−229.7	−601.5	−65.0
3−	AsO_3	679.9	1150.0	−470.1	−822.5	−142.6

[a]SR = steric repulsion, OI = orbital interaction, B = bonding energy, sol = solvation; energies are in kcal·mol^{-1}.

The three negatively charged species $[AsO_3]^{3-}$ display larger endothermic interactions. Also, the ΔE_B term is dominated by the ΔE_{SR} contribution, which accounts for the electrostatic and steric repulsion. It is worth mentioning that, among the dianions, the largest tellurium derivative displays the highest steric and electrostatic repulsion (+806.3 kcal·mol^{-1}) and the largest exothermic orbital contribution (−322.4 kcal·mol^{-1}). This results in a lower endothermic binding energy, which means that the bonding ability is controlled by the ΔE_{OI} such that the trend $[TeO_3]^{2-} > [SeO_3]^{2-} > [HPO_3]^{2-}$ is followed. It should be noted that this energy decomposition analysis is computed without considering any solvation effects. When we take both energies into account, the whole process is significantly more exothermic as shown by the total energies of −94.3, −71.8, and −65.0 kcal·mol^{-1} for $[TeO_3]^{2-}$, $[SeO_3]^{2-}$, and $[HPO_3]^{2-}$, respectively. In other words, the calculations suggest that the selective self-sorting originates from the anion templating effect in solution. In the presence of mixed XY groups, it is more favorable for the $[WO_4]^{2-}$ building blocks to assemble around the $[TeO_3]^{2-}$ and $[SeO_3]^{2-}$ templates rather than that of $[HPO_3]^{2-}$, which would lead to the $[HPO_3]^{2-}$ subsequently occupying the uncapped end of the $\{XYW_{15}\}$ species. This means that the cross-shaped molecules represent kinetic traps for the dopant atom positions and the self-assembly process governs the final architecture.

3.3. Electronic Property Investigations of Mixed-HA Templated Cross-Shaped Polyanions. To understand the electronic properties of the compounds, electrochemical experiments were carried out. The electrochemical reduction of the four cross-shaped POM clusters was investigated in lithium acetate buffer solution (pH 4.3) by differential pulse voltammetry (DPV) and cyclic voltammetry (CV) measurements (Figure 4a and Figure S10). DPV was adopted to gain a more precise understanding of faradaic reduction process of these compounds by avoiding the influence of the capacitance effect on the working electrode. All the reduction potentials are listed in Table S7. As indicated in crystallographic analysis, the size of the external frameworks is nearly identical throughout the cross-shaped molecule family; therefore, the reduction trends observed are fully dependent on the features from the HAs. All four compounds exhibit two sets of reduction waves, which can be assigned as the redox process of $W^{VI} \rightarrow W^{V}$.[14] The $\mathbf{As_4P_4}$ cluster exhibits the most negative set of reduction potentials. This is because the embedded $[AsO_3]^{3-}$ heteroanions are more negatively charged than the $[HPO_3]^{2-}$, $[SeO_3]^{2-}$, and $[TeO_3]^{2-}$, giving a higher negative charge overall of −36, compared to the other three clusters. Therefore, the $\mathbf{As_4P_4}$ is the most difficult compound to be reduced. The

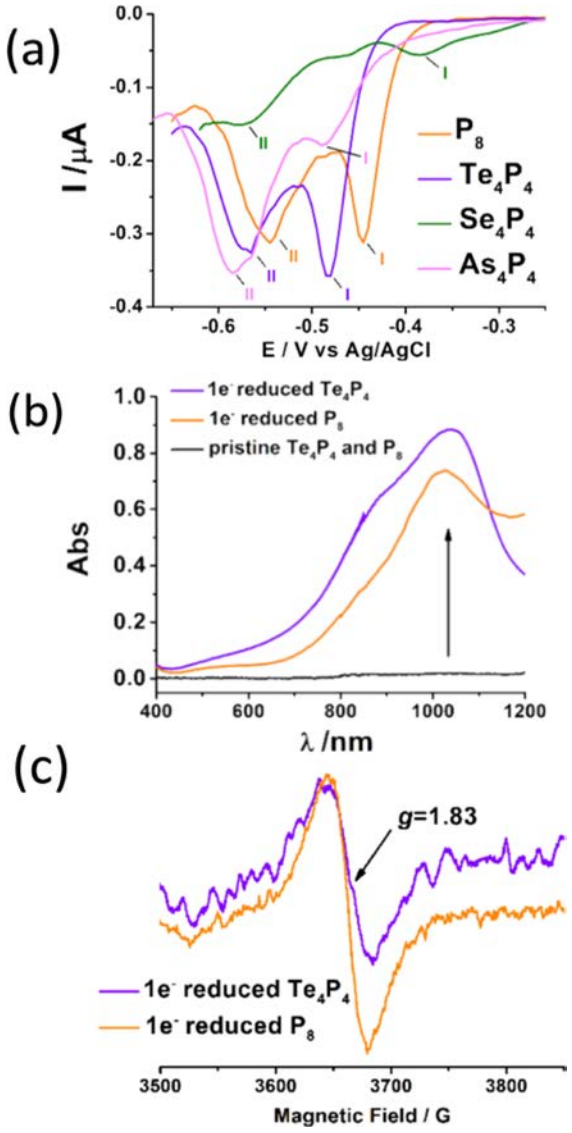

Figure 4. (a) DPVs of cross-shaped POMs in lithium acetate buffer (pH 4.3). (b) UV–vis spectra of one-electron reduction of $\mathbf{Te_4P_4}$ and $\mathbf{P_8}$ ranging from 400 to 1200 nm. (c) EPR spectrum of one-electron reduced $\mathbf{Te_4P_4}$ and $\mathbf{P_8}$.

DOI: 10.1021/jacs.7b11982
J. Am. Chem. Soc. 2018, 140, 2595–2601

remaining set of the molecules all have the same overall negative charge of −32. Among them, $\mathbf{Te_4P_4}$ is the most difficult compound to be reduced, as indicated by the more negative shift of redox potential in both the first and second peaks compared with $\mathbf{Se_4P_4}$ and $\mathbf{P_8}$ (Figure 4a and Figure S10).

In order to understand the electronic properties of the cross-shaped compounds, bulk reductive electrolysis was performed to inject one electron into the $\mathbf{P_8}$ and $\mathbf{Te_4P_4}$. The UV−vis absorption spectra of one-electron reduced $\mathbf{P_8}$ and $\mathbf{Te_4P_4}$, and nonreduced clusters are shown in Figure 4b. Both of the one-electron reduced compounds show a broad absorption centered at 1035 nm, indicating the formation of reduced W^V species. The reduced species were also analyzed by electron paramagnetic resonance (EPR). As shown in Figure 4c, broad signals with a g value of 1.83 were observed, and this indicates the formation of a delocalized W^V species.[34] EPR data are in good agreement with the nature of the frontier orbitals for the compounds (Figure S12), and as expected in POMs, the LUMO of all four clusters is delocalized around the unoccupied tungsten d-like orbitals (Tables S10−S11, Figure S12).

4. CONCLUSIONS

In summary, we have demonstrated positional control of the HAs within the nanosized cross-shaped polyanions $[(XY\text{-}W_{15}O_{54})_4(WO_2)_4]^{32-/36-}$ (X = H−P^{III}, Y= Se^{IV}, Te^{IV}, As^{III}). The position of the HAs has been determined by single crystal X-ray diffraction, NMR spectroscopy, and electrospray ionization mass spectrometry, confirming that mixed HA templated cross-shaped molecules are the preferred self-sorting products crystallizing from the solution. Theoretical analysis using DFT calculations suggested that the highly selective self-sorting originated from the HA templating effects in solution, in which $[WO_4]^{2-}$ anions can more favorably assemble around the bigger $[TeO_3]^{2-}$, $[SeO_3]^{2-}$, and $[AsO_3]^{3-}$, leading to the smaller $[HPO_3]^{2-}$ subsequently occupying the uncapped end of the $\{W_{15}\}$ building blocks. The cross-shaped POM clusters are redox-active, as illustrated by the electrochemical analysis UV−vis spectroscopy and EPR analysis. The differential pulse voltammetry (DPV) experiments clearly showed that the reduction potentials of the molecules can be directly modulated by the embedded HAs. These results indicated that these cross-shaped clusters, with different HAs, may be used to design new nanoscale molecular architectures that are electronically active. In future work, we will aim to increase the differences in redox activity between the different compounds and also explore how they might be used on surfaces to develop new types of hybrid devices to study their charge transport properties.[24]

■ ASSOCIATED CONTENT

Supporting Information

The Supporting Information is available free of charge on the ACS Publications website at DOI: 10.1021/jacs.7b11982.

Detailed crystallography, NMR spectroscopy, mass spectrometry, DFT calculations (PDF)
Crystallographic data (CIF)
Crystallographic data (CIF)
Crystallographic data (CIF)
Crystallographic data (CIF)

■ AUTHOR INFORMATION

Corresponding Authors

*Lee.Cronin@glasgow.ac.uk
*josepmaria.poblet@urv.cat

ORCID

Jia-Jia Chen: 0000-0003-1044-7079
Josep M. Poblet: 0000-0002-4533-0623
Leroy Cronin: 0000-0001-8035-5757

Notes

The authors declare no competing financial interest.

■ ACKNOWLEDGMENTS

The authors gratefully acknowledge financial support from the EPSRC (grant nos. EP/H024107/1, EP/J015156/1, EP/K023004/1, EP/L023652/1, ERC (project 670467 SMART-POM). We also acknowledge financial support from Spanish Ministry of Science and Innovation (grant CTQ2014-52774-P), the DGR of the Generalitat de Catalunya (grant 2014SGR199), and the ICREA foundation (ICREA ACADEMIA). We would also like to thank Dr. Christoph Busche of University of Glasgow for assistance with EPR measurement and Dr. Sergey Zalesskiy of University of Glasgow for the help with temperature-variable NMR measurement and the data analysis.

■ REFERENCES

(1) Love, J. C.; Estroff, L. A.; Kriebel, J. K.; Nuzzo, R. G.; Whitesides, G. M. *Chem. Rev.* **2005**, *105*, 1103.
(2) Kumar, J.; Tsumatori, H.; Yuasa, J.; Kawai, T.; Nakashima, T. *Angew. Chem., Int. Ed.* **2015**, *54*, 5943.
(3) Arduini, A.; Bussolati, R.; Credi, A.; Secchi, A.; Silvi, S.; Semeraro, M.; Venturi, M. *J. Am. Chem. Soc.* **2013**, *135*, 9924.
(4) Schmittel, M. *Chem. Commun.* **2015**, *51*, 14956.
(5) Saha, M. L.; Schmittel, M. *Org. Biomol. Chem.* **2012**, *10*, 4651.
(6) Safont-sempere, M. M.; Fernández, G.; Würthner, F. *Chem. Rev.* **2011**, *111*, 5784.
(7) Whitesides, G. M.; Grzybowski, B. *Science* **2002**, *295*, 2418.
(8) Long, D.-L.; Burkholder, E.; Cronin, L. *Chem. Soc. Rev.* **2007**, *36*, 105.
(9) Baker, L. C. W.; Glick, D. C. *Chem. Rev.* **1998**, *98*, 3.
(10) Proust, A.; Matt, B.; Villanneau, R.; Guillemot, G.; Gouzerh, P.; Izzet, G. *Chem. Soc. Rev.* **2012**, *41*, 7605.
(11) Vilà-Nadal, L.; Cronin, L. *Nat. Rev. Mater.* **2017**, *2*, 17054.
(12) Yin, P.; Li, D.; Liu, T. *Chem. Soc. Rev.* **2012**, *41*, 7368.
(13) Kozhevnikov, I. V. *Chem. Rev.* **1998**, *98*, 171.
(14) Sadakane, M.; Steckhan, E. *Chem. Rev.* **1998**, *98*, 219.
(15) Mizuno, N.; Misono, M. *Chem. Rev.* **1998**, *98*, 199.
(16) Gao, N.; Sun, H.; Dong, K.; Ren, J.; Duan, T.; Xu, C.; Qu, X. *Nat. Commun.* **2014**, *5*, 3422.
(17) Rhule, J. T.; Hill, C. L.; Judd, D. a.; Schinazi, R. F. *Chem. Rev.* **1998**, *98*, 327.
(18) Li, M.; Xu, C.; Wu, L.; Ren, J.; Wang, E.; Qu, X. *Small* **2013**, *9*, 3455.
(19) Clemente-Juan, J. M.; Coronado, E.; Gaita-Ariño, A. *Chem. Soc. Rev.* **2012**, *41*, 7464.
(20) Newton, G. N.; Yamashita, S.; Hasumi, K.; Matsuno, J.; Yoshida, N.; Nihei, M.; Shiga, T.; Nakano, M.; Nojiri, H.; Wernsdorfer, W.; Oshio, H. *Angew. Chem., Int. Ed.* **2011**, *50*, 5716.
(21) Zheng, S.-T.; Yang, G.-Y. *Chem. Soc. Rev.* **2012**, *41*, 7623.
(22) Nishimoto, Y.; Yokogawa, D.; Yoshikawa, H.; Awaga, K.; Irle, S. *J. Am. Chem. Soc.* **2014**, *136*, 9042.
(23) Vasilopoulou, M.; Douvas, A. M.; Palilis, L. C.; Kennou, S.; Argitis, P. *J. Am. Chem. Soc.* **2015**, *137*, 6844.
(24) Busche, C.; Vilà-Nadal, L.; Yan, J.; Miras, H. N.; Long, D.-L.; Georgiev, V. P.; Asenov, A.; Pedersen, R. H.; Gadegaard, N.; Mirza, M. M.; Paul, D. J.; Poblet, J. M.; Cronin, L. *Nature* **2014**, *515*, 545.
(25) Volatron, F.; Noel, J. M.; Rinfray, C.; Decorse, P.; Combellas, C.; Kanoufi, F.; Proust, A. *J. Mater. Chem. C* **2015**, *3*, 6266.
(26) Li, Z.; Li, X.-X.; Yang, T.; Cai, Z.-W.; Zheng, S.-T. *Angew. Chem., Int. Ed.* **2017**, *56*, 2664.

DOI: 10.1021/jacs.7b11982
J. Am. Chem. Soc. 2018, 140, 2595−2601

(27) Niu, J.; Pengtao, M.; Niu, H.; Li, J.; Zhao, J.; Song, Y.; Wang, J. *Chem. - Eur. J.* **2007**, *13*, 8739.
(28) Zhao, J. W.; Jia, H. P.; Zhang, J.; Zheng, S. T.; Yang, G. Y. *Chem. - Eur. J.* **2007**, *13*, 10030.
(29) Wu, Y.; Shi, R.; Wu, Y.-L.; Holcroft, J. M.; Liu, Z.; Frasconi, M.; Wasielewski, M. R.; Li, H.; Stoddart, J. F. *J. Am. Chem. Soc.* **2015**, *137*, 4111.
(30) Müller, A.; Gouzerh, P. *Chem. Soc. Rev.* **2012**, *41*, 7431.
(31) Long, D.-L.; Tsunashima, R.; Cronin, L. *Angew. Chem., Int. Ed.* **2010**, *49*, 1736.
(32) Cadot, E.; Sokolov, M. N.; Fedin, V. P.; Simonnet-Jegat, C.; Floquet, S.; Secheresse, F.; Simonnet-Jégat, C.; Floquet, S.; Sécheresse, F. *Chem. Soc. Rev.* **2012**, *41*, 7335.
(33) Banerjee, A.; Bassil, B. S.; Röschenthaler, G.-V.; Kortz, U. *Chem. Soc. Rev.* **2012**, *41*, 7590.
(34) Vilà-Nadal, L.; Peuntinger, K.; Busche, C.; Yan, J.; Lüders, D.; Long, D.-L.; Poblet, J. M.; Guldi, D. M.; Cronin, L. *Angew. Chem., Int. Ed.* **2013**, *52*, 9695.
(35) Chen, W. C.; Li, H. L.; Wang, X. L.; Shao, K. Z.; Su, Z. M.; Wang, E. B. *Chem. - Eur. J.* **2013**, *19*, 11007.
(36) Stowe, A. C.; Nellutla, S.; Dalal, N. S.; Kortz, U. *Eur. J. Inorg. Chem.* **2004**, *2004*, 3792.
(37) Fleming, C.; Long, D.-L.; McMillan, N.; Johnston, J.; Bovet, N.; Dhanak, V.; Gadegaard, N.; Kögerler, P.; Cronin, L.; Kadodwala, M. *Nat. Nanotechnol.* **2008**, *3*, 229.
(38) Zheng, Q.; Vilà-Nadal, L.; Busche, C.; Mathieson, J. S.; Long, D.-L.; Cronin, L. *Angew. Chem.* **2015**, *127*, 8006.
(39) Busche, C.; Vilà-Nadal, L.; Yan, J.; Miras, H. N.; Long, D.-L.; Georgiev, V. P.; Asenov, A.; Pedersen, R. H.; Gadegaard, N.; Mirza, M. M.; Paul, D. J.; Poblet, J. M.; Cronin, L. *Nature* **2014**, *515*, 545.
(40) Uehara, K.; Miyachi, T.; Nakajima, T.; Mizuno, N. *Inorg. Chem.* **2014**, *53*, 3907.
(41) Wille, H.; Shanmugam, M.; Murugesu, M.; Ollesch, J.; Stubbs, G.; Long, J. R.; Safar, J. G.; Prusiner, S. B. *Proc. Natl. Acad. Sci. U. S. A.* **2009**, *106*, 3740.
(42) Kortz, U.; Savelieff, M. G.; Abou Ghali, F. Y.; Khalil, L. M.; Maalouf, S. A.; Sinno, D. I. *Angew. Chem., Int. Ed.* **2002**, *41*, 4070.
(43) Haouas, M.; Mbomekalle, I.; Vila, N.; de Oliveira, P.; Taulelle, F. *Inorg. Chem.* **2014**, *53*, 5568.
(44) Eda, K.; Maeda, S.; Himeno, S.; Hori, T. *Polyhedron* **2009**, *28*, 4032.
(45) Maeda, S.; Goto, T.; Takamoto, M.; Kazuo, E.; Himeno, S.; Takahashi, H.; Hori, T. *Inorg. Chem.* **2008**, *47*, 11197.
(46) Gao, J.; Yan, J.; Beeg, S.; Long, D.-L.; Cronin, L. *Angew. Chem., Int. Ed.* **2012**, *51*, 3373.
(47) Karunanithy, G.; Cnossen, A.; Müller, H.; Peeks, M. D.; Rees, N. H.; Claridge, T. D. W.; Anderson, H. L.; Baldwin, A. J. *Chem. Commun.* **2016**, *52*, 7450.
(48) Brutscher, B. *Concepts Magn. Reson.* **2000**, *12*, 207.
(49) López, X.; Carbó, J. J.; Bo, C.; Poblet, J. M. *Chem. Soc. Rev.* **2012**, *41*, 7537.

DOI: 10.1021/jacs.7b11982
J. Am. Chem. Soc. 2018, 140, 2595−2601